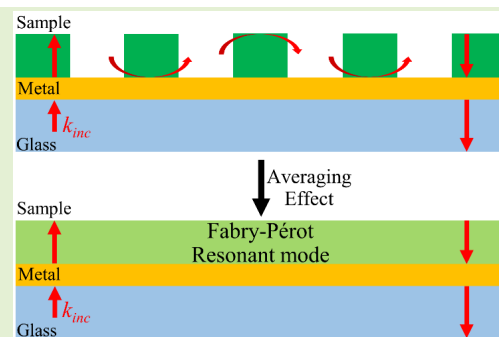# Analysis of Open Grating-Based Fabry–Pérot Resonance Structures With Potential Applications for Ultrasensitive Refractive Index Sensing

Suvicha Sasivimolkul, Suejit Pechprasarn, and Michael G. Somekh

Abstract—We report a theoretical framework to explain the characteristics of Fabry-Pérot (FP) resonances excited in a thin film-based grating consisting of a thin gold layer and a rectangular dielectric grating in the sub-wavelength and near-wavelength grating regimes. The zeroth-order diffraction inside the grating layer forms an FP resonant cavity with effective refractive index arising from an averaging effect between the refractive indices of the grating material and the filling material between the grating grooves. A simplified model based on Fresnel equations and phase matching condition is proposed to predict the FP resonant mode for the grating structure, this is compared with rigorous coupled-wave analysis to determine its range of validity. We also compare the performance of the proposed structure with other thin film-based interferometers for refractive index sensing applications, in terms of, sensitivity, full width at half maximum, figure of merit and dynamic range. The proposed structure has a full width at half maximum around 10 times to 60 times narrower than conventional surface plasmon resonance and conventional FP resonators. Thus, the figure of merit is higher than Kretschmann based surface plasmon resonance and FP structures by a factor of 20 and 2 respectively with a wider dynamic range. The total energy stored in the grating resonant cavity is 5 and 20-fold greater than the surface plasmon resonance configuration and the conventional FP structures. Since the resonator discussed here is an open structure, it is far better suited for liquid sensing compared to a closed FP structure.

Index Terms—Optical sensors, biosensors, Fabry-Pérot, optical resonators, subwavelength grating.

Suvicha Sasivimolkul is with the College of Biomedical Engineering, Rangsit University, Pathum Thani 12000, Thailand (e-mail: suvicha.sa61@rsu.ac.th).

Suejit Pechprasarn is with the College of Biomedical Engineering, Rangsit University, Pathum Thani 12000, Thailand, and also with the Shenzhen Key Laboratory for Micro-Scale Optical Information Technology, Nanophotonics Research Center, Institute of Microscale Optoelectronics, Shenzhen University, Shenzhen 518060, China (e-mail: suejit@szu.edu.cn).

Michael G. Somekh is with the Shenzhen Key Laboratory for Micro-Scale Optical Information Technology, Nanophotonics Research Center, Institute of Microscale Optoelectronics, Shenzhen University, Shenzhen 518060, China, and also with the Faculty of Engineering, University of Nottingham, Nottingham NG7 2RD, U.K. (e-mail: michael.somekh@nottingham.ac.uk).

Digital Object Identifier 10.1109/JSEN.2021.3063136

I. Introduction

MANY sensors operate as resonators with the analyte perturbing the resonant conditions. The effect of this is depicted in a highly generalized form in Fig. 1(a). The y-axis shows the response of a resonator (this can be optical reflectivity, transmission, or even the optical phase) plotted against the resonance position; again, the parameter that records the change in the resonance can be, for instance, wavelength or angle. A good sensor will, in general, have a high sensitivity, which means that for a given change in analyte properties, the resonance position will move by a considerable distance. Moreover, the resonance should also be sharp so that small movements of the resonance position may be resolved. These qualitative considerations will be defined more formally later in the paper.

For instance, a FP resonator, as depicted in Fig. 1(b) can detect very small changes in the refractive index by sensitive detection of optical path length changes [1]. A resonant cavity using Bragg reflectors [2], as shown in Fig. 1(c) can have even better performance with a sharper response since the ohmic losses are significantly reduced [3]. In these types of closed
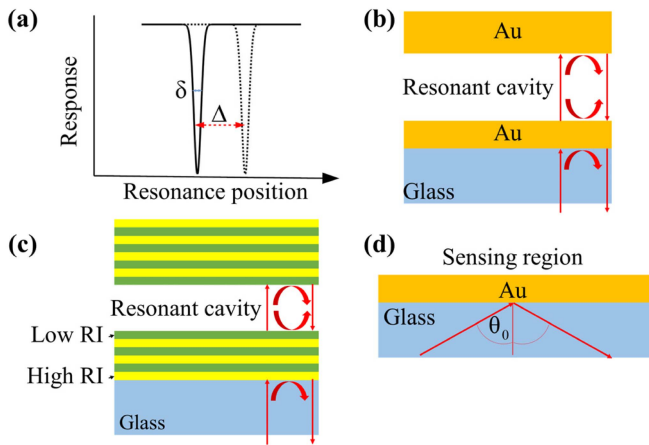
Fig. 1. (a) Generalized responses of an optical sensor. And three schemes for (b) FP resonator (c) Bragg reflectors and (d) Kretschmann configuration.

Fig. 2. Scheme of the open grating-based FP resonator.

resonator structures, the analyte becomes an integral part of the resonant structure, which means that it is possible to have a very large change in the resonant position while retaining the sharp response.

The problem with closed resonator structures, such as the FP resonator, is the very fact that they are closed, which makes access to a liquid analyte relatively inconvenient. This is especially problematic when the separation between the reflectors is very small, as it is for some of the most sensitive sensors [1]. A surface plasmon (SP) sensor provides convenient access to the analyte since it is external to the surface plasmon sensor. The SP sensor with the Kretschmann configuration is shown in Fig. 1(d). Although it is not so immediately obvious, an SP sensor can also be regarded as a resonator structure [4]; however, in this case, the analyte acts like an external perturbation to the resonator. A detailed analysis of the resonance conditions for SP sensors are given in [4], broadly speaking, external perturbation of a resonator corresponds to small changes in the properties of the reflecting mirrors. In contrast, internal perturbation involves changes in the properties of the resonant cavity see, for instance, Fig. 1(a) or Fig. 1(b). With an external perturbation, the sharpness of the resonance and the change in resonant position with perturbation by an analyte are strongly linked, so a large change in resonance position is associated with a broad resonance for a specific material system [4]. Internal perturbation breaks this link.

For sensing applications, such as refractive index sensors for gas and liquid, SP sensors [5], [6] are preferable over FP sensors [7] since conventional FP sensors require sophisticated channel fabrication. Although it is well established that SP [3] requires a higher incident light momentum for excitation and the coupling process usually gives a broader resonance dip at a larger wave vector position compared to the FP resonators. The easy access of the analyte in SP sensors compared to conventional FP sensors means that they are preferred for most applications.

Fig. 2 shows the structure of the open resonator we study in this paper. It consists of a thin metal film which is overlaid which an 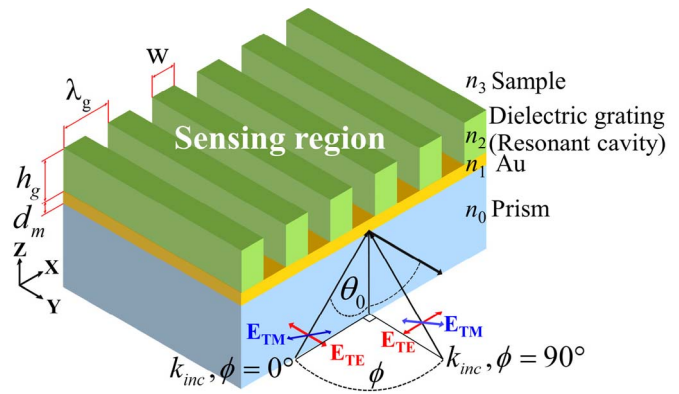open dielectric grating. Since the grating is an open structure the analyte can fill the gaps in the dielectric, thus forming part of the grating. The grating region fulfills the role of the resonant cavity, so when the analyte fills the cavity the properties of this region change, the structure thus responds to both internal and external perturbation. It is, however, the internal perturbation that confers the new and exciting properties on the structure. It should be pointed out that this structure appears somewhat similar to a Kretschmann type structure, with the illumination path and the analyte conveniently separated. However, although SPs can be excited in this structure, the most effective sensors do not employ plasmonic excitation, and indeed very effective sensing can also be realized with TE polarization.

The open resonator structure we present thus combines the advantages of an open resonator with internal perturbation. This type of structure provides easy access to the analyte and breaks the trade-off between the sharpness of the resonance and the change in the resonant position associated with external resonator structures.

This paper is divided into five parts, and section II explains device parameters and analysis framework. Section III examines the resonant mode. Section IV analyses its performance for refractive index sensing and analyses its field distribution and field enhancement. Section V discusses device fabrication feasibility and considers the effects of changes in measurement conditions.

II. DEVICE STRUCTURE AND ANALYSIS FRAMEWORK

The open grating-based FP resonator in Fig. 2 consists of 4 layers: a prism, a thin gold layer, a dielectric grating, and sample. Polydimethylsiloxane (PDMS) was chosen as the grating material because of its transparency and biocompatibility [8]. The layer refractive indices were $n_0 = 1.52$, $n_1 = 0.18344 + 3.4332i$ [9], $n_2 = 1.4283$ [10] and $n_3 = 1.00$ respectively. Note that the sample is air (1.00) through section III. The incident light to the structure is linearly polarized at 633 nm wavelength (λ_0). A HeNe laser can provide stable optical output, usually employed in SP measurements [11]. However, the device is not limited to this wavelength and is applicable to other coherent sources. Since different polarizations have different responses as discussed later one may use either TE or TM polarization.
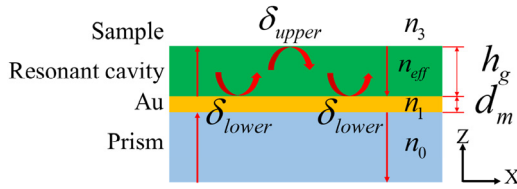
Fig. 3. A simplified model of the open grating-based FP resonator.

Fig. 4. Refractive index contrast (Δn) between grating material and sample ranging from 0.5 to 3.0 (0.5 steps) and varying λ_g of $0.1\lambda_0$ to $2.0\lambda_0$ in TM polarization with d_m of 48 nm, h_g of $10\lambda_0$, n_2 of 1.5 to 4.0 (0.5 steps), n_3 of 1.00 and $\phi = 0$.

Fig. 2 shows the following parameters: d_m is the gold thickness, h_g is the grating thickness, λ_g is the grating period, w is the width of the stripe and the fill factor (*FF*) is defined as the width of stripe over the grating period, w/λ_g. A plane wave illumination to the structure is defined by incident angle θ_0 in the plane of incidence. The azimuthal angle ϕ determines the plane of incidence relative to the grating vector. For $\phi = 0°$, the grating vector is in the plane of incidence, and for $\phi = 90°$, the grating vector is perpendicular to the plane of incidence. TM or TE polarization refers to the input polarization relative to the plane of incidence.

In this work, two calculation methods were used. (i) Fresnel equations with the transfer matrix method [12], this is an approximate method to calculate the position of the FP modes. Under certain conditions the FP modes inside the dielectric grating can be modelled with this simplified approach by replacing the grating layer with a uniform layer having an effective refractive index (n_{eff}) [13], [14] as shown in (1) and shown in Fig. 3. (ii) rigorous coupled-wave analysis [15] (RCWA) for computing responses of grating structures. Note that all the results calculated using RCWA in this paper used 81 orders and were tested for convergence. The software in (i) and (ii) have been developed in house under MATLAB utilizing parallel computing capability [16].

$$\varepsilon_{eff}^2 = n_{eff} = \sqrt{n_2^2 FF + n_3^2(1 - FF)} \qquad (1)$$

where ε_{eff} is the permittivity of the effective medium of the FP resonant cavity, n_2, n_3 and *FF* are as defined above.

The approximate method is essentially effective medium theory where the structure can be considered to support a single Bloch mode [17]. In this simplified model the structure is effectively an asymmetric FP cavity [18], [19], whose resonances can be described by the following mode condition, as shown in (2).

$$2k_{z,cavity}h_g + \delta_{upper} + \delta_{lower} = 2\pi M \qquad (2)$$

where δ_{upper} is the phase angle of reflection coefficient at the upper interface of an effective medium, δ_{lower} is the phase angle of reflection coefficient at the lower interface of an effective medium as depicted in Fig. 3 and M for the Mth mode of the FP resonant modes and $k_{z,cavity}$ is the wave vector along z axis inside the effective medium and expressed in (3).

$$k_{z,cavity} = \sqrt{\left[\frac{2\pi}{\lambda_0}n_{eff}\right]^2 - \left[\frac{2\pi}{\lambda_0}n_0\sin\theta_0\cos\phi + K_g\right]^2} \qquad (3)$$

where K_g is the product of the grating wave vector and the diffraction order, m, so it is given by $m2\pi/\lambda_g$
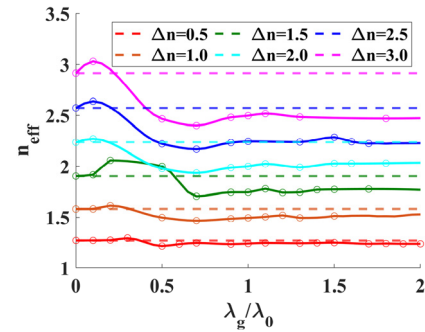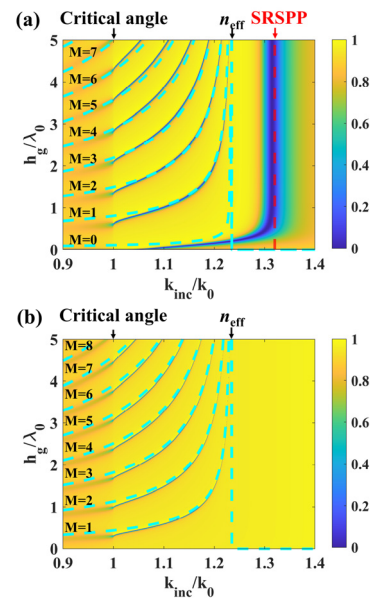

Fig. 5. The effect of varying grating thickness on reflectance response for (a) TM polarization with d_m of 48 nm and (b) TE polarization with d_m of 38 nm. Dashed cyan curves show the wave vector positions satisfying (2). With λ_g of $0.1\lambda_0$, *FF* of 0.5, n_3 of 1.00 and $\phi = 0$. Note that curves are calculated with (2), contours are calculated with RCWA.

The range of validity of the Fresnel equations (or effective medium theory) needs to be considered. (1) determines the effective refractive indices. This value also gives a FP resonant mode cut-off position, as shown with the labels 'n_{eff}' in Figs. 5 this may be compared with the actual mode positions calculated by RCWA for different refractive index contrasts ranging from 0.5 to 3.0, as shown in Fig. 4. The refractive index contrast (Δn) is the difference between the grating material index and sample index; $\Delta n = n_2 - n_3$. The dashed lines are the effective refractive indices calculated from (1), which are constant. The solid curves show the FP mode cut-off positions calculated by RCWA. For the grating period of $0.1\lambda_0$, the approximation can identify the mode cut-off position and give similar results compared to the RCWA calculation. However, when the grating period increases, the mode positions predicted by the approximate model deviate from the mode positions calculated using RCWA, especially for the higher refractive index contrast cases. It can be seen that the

approximate method is valid over all the simulated grating periods when the refractive index contrast is less than 1.0 and is not suitable to account for the response of gratings with high contrast [20]. In this situation more than one Bloch mode participate and interfere, so the effective medium approach breaks down. This conforms to an intuition where one might expect that the validity of the Fresnel model to be less good when the diffracted orders are not evanescent or put more precisely when more than one Bloch mode is propagating.

Note that, when the situation is approximated with the Fresnel equations, one can only expect consistent responses for 0th order diffraction, however, if the effective medium theory is applicable one may determine modal position of diffracted curves, even though the model cannot predict the values of reflectivity and transmissivity in these cases. In section IV we give an example where dispersion modes corresponding to values of $m \neq 0$ may be predicted by substituting the appropriate value of $k_{z,cavity}$ into (2).

III. ANALYSIS OF RESONANT MODES

Fig. 5(a) and Fig. 5(b) show simulated 0th order diffraction reflectance responses, using RCWA, which has the strongest diffraction efficiency, for an incident beam with TM polarization ($|r_p|^2$) and TE polarization ($|r_s|^2$). The mode positions for the FP resonances calculated using the effective medium are overlaid in these figures as the dashed lines. The gold thickness of 48 nm for the TM polarization and 38 nm for TE polarization were chosen as a value that gives the strongest reflectivity contrast for each polarization at FP resonance when the sample is air. Several FP modes occur at different grating thicknesses for both TM and TE polarizations. The higher grating thicknesses introduce higher-order FP modes resulting from the increasing optical path length. To form a FP cavity, the grating diffracted orders must form propagating waves inside the grating. The critical angle k_{inc}/k_0 of the structure is highlighted as 'Critical angle' in Fig. 5(a) and Fig.5(b).

Incident wave vectors greater than the critical angle provide the strongest back reflection through total internal reflection at the boundary between the grating and the sample. The FP resonances below the critical angle are weakly coupled due to the low Q of the cavity. It can be seen that just above the critical angle there is a larger discrepancy between the modal positions calculated from the Fresnel resonance and those calculated by RCWA, this is because just above the critical angle there is some leakage of radiation into the air, whereas at larger incident angles the approximation of total internal reflection at the grating/air interface is much better. There is also a mode cut-off for the FP modes occurring at the incident wave vector labeled as 'n_{eff}' as shown in the figures. Above this incident angle the effective medium does not support propagating modes for the 0th order, so the structure does not function as a resonant cavity, so the FP approximation breaks down. Using (1) the value of n_{eff} when the 0th order becomes evanescent is 1.2329.

The wave vector of each mode can be approximated using (1) and (2). Dashed cyan curves shown in Fig. 5(a) and Fig. 5(b) are the k-vector positions for FP cavity modes with M of 0 to 8. The M value of 0 can only exist in the
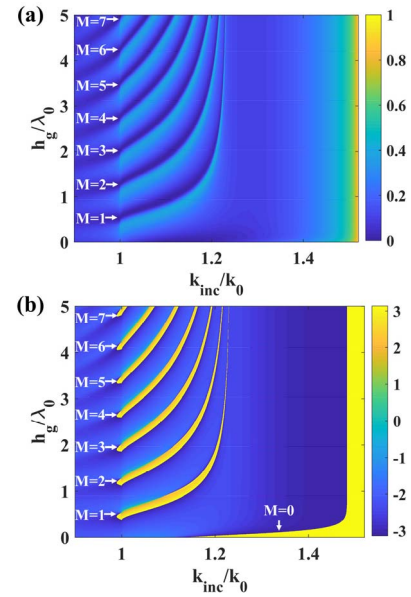

Fig. 6. (a) Reflectance response and (b) phase response of TM polarization incident wave with $n_1 = 0.7936 + 0.7936i$, λ_g of $0.1\lambda_0$, FF of 0.5, n_3 of 1.00 and $\phi = 0$.

TM polarization since the 0th order solution to Maxwell's equations of planar waveguide structure is only valid for the TM polarization [21], [22].

To explain the $M = 0$ FP mode, let us suppress the effect of surface plasmons (SP) by setting the real part of the complex permittivity of gold ε_1 to zero. It is well established that the plasmonic effect requires a negative real part of the complex permittivity, such as found in noble metals at visible wavelengths [9]. The complex permittivity of gold is n_1^2, which is $-11.7532 + 1.2596i$ to suppress the possibility of generating plasmons the real part is set to zero, the permittivity becomes $\sqrt{1.2596i}$ or $0.7936 + 0.7936i$. Fig. 6(a) shows $|r_p|^2$ for n_1 of $0.7936 + 0.7936i$ and Fig. 6(b) shows the corresponding phase of r_p. It is clear that the plasmonic effect is suppressed, but the 0th order FP mode ($M = 0$) can still be excited. The cut-off for the mode occurs at k_{inc}/k_0 of 1.52, whereas the other higher orders have their mode cut-off at k_{inc}/k_0 of n_{eff}. In other words, the higher-order FP modes require a propagating wave to form a resonance, whereas the 0th order mode ($M = 0$) can be formed by both propagating wave and evanescent wave [23]. Similar curves would be obtained if a metal that does not support SP excitation such as chromium were used instead of the artificial material value used here.

The dashed red curve in Fig. 5(a) shows the wave vector of the short-range surface plasmon polariton (SRSPP), which can only be excited with TM polarization and can be calculated by the surface plasmon dispersion relation as shown in (4) [16].

$$k_{SRSPP} = \frac{2\pi}{\lambda_0} n_0 \sin \theta_0 = \frac{2\pi}{\lambda_0} \sqrt{\frac{\varepsilon_m \varepsilon_{eff}}{\varepsilon_m + \varepsilon_{eff}}} \qquad (4)$$

In this work, the grating material is chosen as low index material (that is PDMS) so that there is relatively small contrast between the grating material and the filler. When there is a sufficiently large index contrast and a near-wavelength
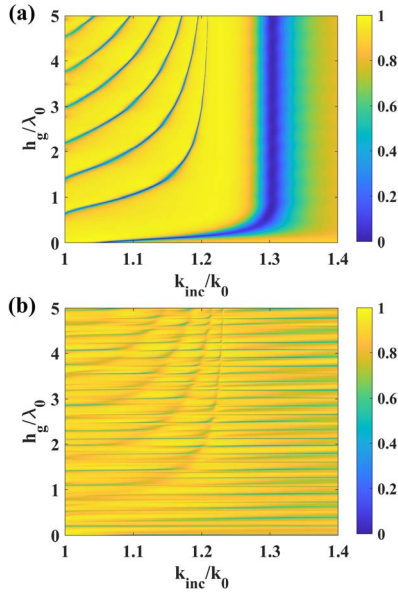
Fig. 7. Reflectance response of TM polarization incident wave for (a) the low-contrast and (b) the high contrast cases with varying h_g, d_m of 48 nm, λ_g of λ_0, FF of 0.5, n_3 of 1.00 and $\phi = 0$.

Fig. 8. Reflectance of TM polarization in function of normalized wave vector (k_{inc}/k_0) with following parameters d_m of 48 nm, h_g of 1 μm, λ_g of 0.1 λ_0, FF of 0.3, n_3 of 1.33 and 1.34 for blue and orange color respectively and $\phi = 0$.

grating period condition more than one Bloch mode is present and the situation strongly deviates from the effective medium condition. To analyze this effect, two sets of grating structures with identical parameters except the refractive index of grating material n_2 were different with the n_2 of 1.4283 and 3.48 for the low contrast and the high contrast cases respectively; varying h_g, d_m of 48 nm, λ_g of λ_0 (near-wavelength condition), fill factor of 0.5, n_3 of 1.00, $\phi = 0$ and TM polarization light. The responses for low and high contrast respectively as shown in Fig. 7. The underlying $m = 0$ patterns show similar structure for both structures but there is increased complexity due the interference between different Bloch modes, which lead to complex behavior with a considerable hybridization. For this reason, we confine our discussion of sensor applications to low contrast structures.

IV. ANALYSIS FOR REFRACTIVE INDEX SENSING, FIELD DISTRIBUTION AND FIELD ENHANCEMENT

Comparative parameters for refractive index sensing are defined as the following:

(i) Bulk sensitivity or refractive index sensitivity (S_{bulk}) is defined as the change in normalized wave vector (k_{inc}/k_0) of FP mode wave vector position over the change refractive index of sample region (n_3), which is expressed as:

$$S_{bulk} = \frac{dk_{inc}/k_0}{dn_3} \quad (5)$$

(ii) Full-width at half-maximum (FWHM) [24] is the wave vector bandwidth of reflectance dip of a mode at reflectance equal to 0.5 as shown in Fig. 8. This value also relates to the minimum detectable change of sample properties.

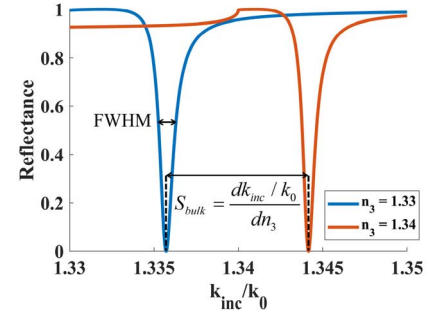(iii) Figure of merit (FoM) is the ratio of sensitivity over FWHM [25]. The FoM is proportional to

Q-factor 24], [26]. To eliminate the redundancy between the two similar quantities, here only FoM is considered.

$$FoM = \frac{S_{bulk}}{FWHM} \quad (6)$$

(iv) Dynamic range (DR) is the numerical value indicating the range of refractive indices, which the sensor can measure under defined conditions; the reflectance at the minimum reflectance dip of a mode must be less than 0.25 [27].

The refractive index sensing capability of the proposed open grating based FP resonator is quantified compared to the conventional FP resonator shown in Fig. 1(b) and Fig. 1(c) and the Kretschmann configuration based surface plasmon resonance sensor shown in Fig. 1(d). Details of the structures were:

(i) Surface Plasmon Resonance (SPR) with Kretschmann configuration (KC) with a gold thickness of 48 nm.

(ii) FP structure with two metallic mirrors consisting of 45 nm gold thin film and 90 nm gold thick film, separated by the FP resonant cavity. The thickness of the cavity is 1.023 μm.

(iii) FP structure with Bragg mirrors consisting of low-index ($n_{low} = 1.37$, MgF$_2$ [28]) and high-index ($n_{high} = 2.40$, TiO$_2$ [29]) materials to form the two Bragg mirrors [30]. The Bragg mirror's top and bottom consist of n_{high}, n_{low},n_{high},n_{low} and n_{high} stacking. The thickness for n_{low} and n_{high} layer are $\lambda_0/(4n_{low})$ and $\lambda_0/(4n_{high})$. The thickness for the cavity is 1.023 μm.

(iv) The open grating FP resonator consisting of d_m of 48 nm for TM polarization and d_m of 38 nm for TE polarization, h_g of 1 μm, λ_g of 1.25λ_0, FF of 0.3

Note that the thickness of the structure (iv) was different from the other two FP structures to ensure that the optical length $2k_{z,cavity}h_g$ were the same for all three structures for a fair comparison. Table I. shows the refractive index sensing performance of the different FP modes with the highest FoM for each structure. For the grating structure, the grating vector lies in the plane of incidence.

The structures (i) (ii) and (iii) have a higher bulk sensitivity around 1.7, 13.4 and 19.3 times compared to the structure (iv) with a fill factor of 0.3. The bulk sensitivity of structure (iv)

TABLE I
COMPARATIVE PARAMETERS OF EACH STRUCTURE

| Structure	Bulk sensitivity [RIU⁻¹]	FWHM	FOM	Dynamic range of n_3
Structure (i) SPR	1.1870	0.0349	34	1.00 − 1.40
Structure (ii) FP	9.0811	0.0248	365	1.23 − 1.36
Structure (iii) FP	13.0490	0.0307	426	1.10 − 1.27
Structure (iv) FP with TM	0.7236	0.0011	680	1.00 − 1.38
Structure (iv) FP with TE	0.6287	0.0006	902	1.00 − 1.35

Fig. 9. Sensing response of proposed structure with TM polarization. (a) FF of 0.3 (b) FF of 0.25 and (c) zoom image (red dashed box in Fig. 9(b)). Other parameters: d_m of 48 nm, h_g of 1 μm and λ_g of 1.25λ_0.

increases as the fill factor decreases. The lower fill factor gives more space for the analyte to fill the groove of the grating so one expects the bulk sensitivity to rise. Moreover, the fill factor of 0.3 provides a clean and uninterrupted response without any hybridization [31], as shown in Fig. 9(a), and compared to Fig. 9(b) in the case where hybridization occurs. For the fill factor of 0.25 there is clear hybridization between the $m = 0$ mode and the $m = -2$ mode, with the same M = 1, this is readily predicted by application of (2) and (3). The designer may therefore use these simple equations as a quick check to ensure that no hybridization response occurs within the desired refractive index range.

The highest bulk sensitivity that can be achieved is around 1.00 RIU⁻¹, where the sensing response dip is parallel to critical angle as shown with pink dashed line in Fig. 9(a). It should be noted that the SP sensitivity for bare gold layer with no grating differs from the grating coated structure, we naturally compare the sensitivity values with bare gold as used in regular SP sensors.

The FWHM of the FP modes in structure (iv) was 30 times narrower than the conventional FP resonator. Thus, the FoM of the structure (iv) was 20 times greater compared to the structure (i) and about 2 times compared to the structure (ii) and structure (iii). The proposed open grating based FP resonator can provide a more extensive operating range combined with high FoM compared to the other structures.

The FP resonant modes occur at an angle below the SRSPP angle, so that this structure also allows us to mitigate the requirement of an ultrahigh numerical aperture (NA) objective lens if the sensor is implemented within a microscope system.

The total normalized intensity $(|\vec{E}_x|^2 + |\vec{E}_y|^2 + |\vec{E}_z|^2)/|\vec{E}_{inc}|^2$ is proportional to the total energy stored in the FP resonant cavity. Figs. 10 shows the total normalized intensity of the grating structure at the wave vectors labeled 'A', 'B', 'C', and 'D' highlighted in Fig. 9(b).

Figs. 10(a) and 10(b) showed the field distribution when the pure FP resonance *M* of 1 was excited, and the field pattern appears as nodes inside the PDMS material and the antinodes in the gap regions [32]. The high stored energy at 'B' compared to 'A' is clearly related to the higher Q that can be observed from the narrow FWHM. Fig. 10(c) shows the field corresponding to the position at hybridization 'C'. It can
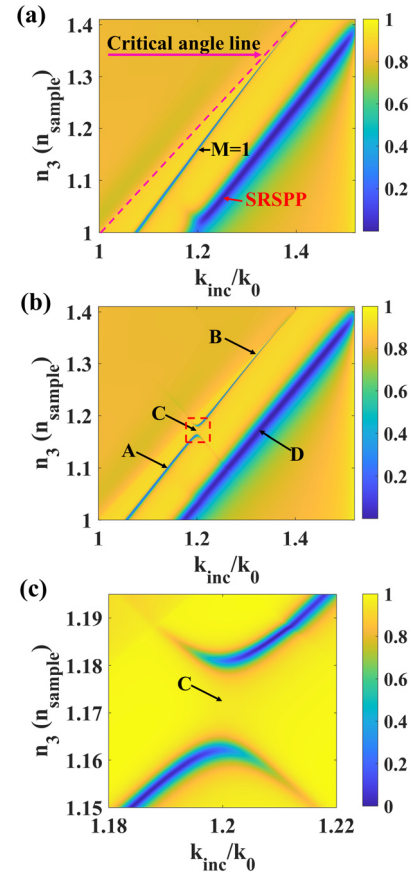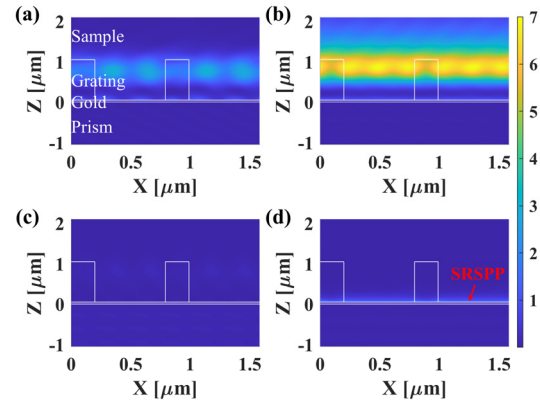
Fig. 10. The total normalized electric field distribution, which normalized by Kretschmann structure. (a), (b), (c) and (d) are corresponding to 'A', 'B', 'C' and 'D' marked points in Fig. 9(b) respectively.

be seen that any standing wave pattern cannot be formed due to the phase cancellation between the two FP modes, the energy stored inside the structure becomes smaller than the two pure FP mode positions 'A' and 'B' and close to zero. Fig. 10(d) shows the field distribution of SRSPP, which was confined on the gold surface. The fields in the FP resonators were also calculated but are not shown from brevity.

In comparison, the total normalized intensity of every structure is normalized by the highest total normalized

intensity of conventional Kretschmann surface plasmon resonance structure, which is the structure (i). Thus, the highest total normalized intensity of the labeled 'A', 'B', 'C', 'D', structures (ii) and structures (ii) are 3.04, 7.00, 0.16, 1.68, 0.18 and 0.34 fold greater compared to the conventional surface plasmon in structure (i), respectively.

V. FEASIBILITY ANALYSIS FOR DEVICE FABRICATION, FABRICATION TOLERANCE AND TOLERANCES TO CHANGES IN EXPERIMENTAL CONDITIONS

Although this paper focuses on theoretical analysis, we suggest some feasible fabrication protocols and analyze fabrication tolerance in this section. The protocols start with depositing 2nm of titanium (Ti) as an adhesion layer and 48 nm of gold (Au) on a cleaned glass substrate using thermal evaporator [33]. A master mold for the grating pattern can be realized by spin coating a 1-micron thick layer of AR-P 672.08 on a cleaned glass substrate at 3,000rpm for 60 seconds before baking on a hot plate at 150 °C for 3 minutes [34]. The coated substrate is then exposed in an electron beam with a current of 3.3nA and a voltage of 80keV. Stitching errors can be minimized by multishot exposure with a total dose of 550μC/cm^2. The sample can be then developed in IPA:MIBK 3:1 for 3 minutes before being rinsed IPA for 1 minute. Finally, the sample baking on a hotplate at 150 °C for 3 minutes improves the strength of the structure. The PDMS can be then stamped on to the cleaned the gold coated substrate using the master mold [35]. Our simulations suggest that almost identical performance to that described in this paper can be achieved with PMMA in which case even more straightforward fabrication will be possible by spinning the photoresist directly onto the gold surface.

Grating parameters and the refractive indices of PDMS and gold were varied to analyze the fabrication tolerance. The criteria for determining the fabrication tolerance are that the sensor with the modified parameters can maintain the sensitivity, the FWHM, and the resonant position within ±5% variation from the theoretical values. For the resonant position, the fabrication tolerances also consider the hybridization to avoid coupling between modes. Table II shows the fabrication tolerance.

The proposed open grating resonator provides convenient access to the sensing region. In an experimental scenario, the sensor can be affected by ambient temperature, humidity, and polluted air unavoidably. These can lead to undesirable effects. The light source also affects the measurement; the optical outputs can fluctuate, resulting in optical power fluctuation and wavelength shift [36]. A reference channel exposed to similar environmental fluctuations can be used to mitigate such variations [37].

However, the power fluctuation would not affect the measurement as the proposed structure measures the variation in the resonant dip position or if a reference channel is used in conjunction with an intensity measurement. The wavelength shift would affect the resonant dip position by 6.3×10^{-4} rad/nm for 1 nm shift in incident wavelength, equivalent to 1.5×10^{-4} RIU of the sample refractive index.

TABLE II
FABRICATION TOLERANCE

Parameter	Fabrication range
h_g	$950 - 1500$ nm
λ_g	$630 - 920$ nm
FF	$0.28 - 0.30$
real part of Au	$0.1 - 0.2$ RIU
imaginary part of Au	$3.00 - 4.3$ RIU
refractive index of PDMS	$1.42 - 1.45$ RIU

The wavelength fluctuation over 5 hours is $\pm 2 \times 10^{-6}$ nm [38], corresponding to a negligible error.

The temperature fluctuation also affects the sensor due to the thermo-optic coefficient of the materials. Lin *et al.* [39] reported the temperature effect on SP sensor with Kretschmann configuration. The dip position shifts to a smaller value. In our case, thermo-optic coefficient of water at 25 °C, PDMS, the real part and the imaginary part of Au are -1×10^{-4} RIU/°C [39], -4.5×10^{-4} RIU/°C [40], 3×10^{-4} RIU/°C [41] and $-1.2 \times 10^{-4}i$ RIU/°C [41], respectively. These refractive indices would account for the change in the resonant dip position by -1.5×10^{-3} rad/nm for 1 °C increase, which is equivalent to 1.8×10^{-4} RIU of the sample refractive index.

For the humidity effect, PDMS is a hydrophobic material that is relatively immune to humidity [42]. Liu *et al.* [43] employed PDMS coating on the sensor surface to isolate the temperature and humidity. Therefore, the proposed structure is expected to be more robust to variation in the humidity. The refractive index of air, taking into account the temperature, the humidity and the pressure can be calculated by equation as proposed by Ciddor [44]. At the standard pressure (1 atm) and room temperature (25 °C), the air's refractive index changes by 1.14×10^{-8} RIU/%RH. This leads to the difference in the resonant position of 1.3×10^{-7} rad/nm and 7.2×10^{-9} rad/nm when %RH increases by 1% for the SP sensor and the proposed open grating, respectively.

VI. CONCLUSION

From a conceptual point of view the present sensor differs from sensors such as an SPR sensors in that the inherent tradeoffs in such systems do not apply in the open resonator structure. In an SPR sensor the gold layer forms the sensor surface only responds to the changes in the external environment (the gold properties themselves do not change) whereas in the present system the resonant structure itself changes with the analyte. In the present system the link between the response to a refractive index changes and the sharpness of the resonance with incident angle is broken allowing significant changes in the resonance position combined with a sharp response thus giving a considerable enhancement in potential sensitivity.

We have studied the optical properties of open grating-based FP resonators with low index grating material. This work provides an approximate method and defines the limit of its validity that allows the grating structure to be analyzed as an FP resonator with an effective medium theory. An intuitive

rule of thumb helps one design a promising sensor whose performance can ultimately be validated with RCWA.

With the open grating design, a sample can easily interact with the sensor at the open space on the top of the structure. It is worth reiterating that the metal layer is here to provide the loss mechanism for the FP modes rather than support surface plasmons. If the metal layer is replaced by a dielectric structure, an even greater sensitivity may be expected if a phase-sensitive detector is used [45].

REFERENCES

[1] M. Shen, S. Learkthanakhachon, S. Pechprasarn, Y. Zhang, and M. G. Somekh, "Adjustable microscopic measurement of nanogap waveguide and plasmonic structures," *Appl. Opt.*, vol. 57, no. 13, pp. 3453–3462, May 2018.

[2] W. Liang, Y. Huang, Y. Xu, R. K. Lee, and A. Yariv, "Highly sensitive fiber Bragg grating refractive index sensors," *Appl. Phys. Lett.*, vol. 86, no. 15, Apr. 2005, Art. no. 151122.

[3] S. Pechprasarn, T. W. Chow, and M. G. Somekh, "Application of confocal surface wave microscope to self-calibrated attenuation coefficient measurement by Goos-Hänchen phase shift modulation," *Sci. Rep.*, vol. 8, no. 1, pp. 1–14, 2018.

[4] M. Shen and M. G. Somekh, "A general description of the performance of surface plasmon sensors using a transmission line resonant circuit model," *IEEE Sensors J.*, vol. 19, no. 23, pp. 11281–11288, Dec. 2019.

[5] P. S. Vukusic, G. P. Bryan-Brown, and J. R. Sambles, "Surface plasmon resonance on gratings as a novel means for gas sensing," *Sens. Actuators B, Chem.*, vol. 8, no. 2, pp. 155–160, May 1992.

[6] B.-H. Liu, Y.-X. Jiang, X.-S. Zhu, X.-L. Tang, and Y.-W. Shi, "Hollow fiber surface plasmon resonance sensor for the detection of liquid with high refractive index," *Opt. Exp.*, vol. 21, no. 26, pp. 32349–32357, 2013.

[7] T. Wei, Y. Han, Y. Li, H.-L. Tsai, and H. Xiao, "Temperature-insensitive miniaturized fiber inline Fabry–Pèrot interferometer for highly sensitive refractive index measurement," *Opt. Exp.*, vol. 16, no. 8, pp. 5764–5769, 2008.

[8] D. Wang *et al.*, "A novel approach for PDMS thin films production towards application as substrate for flexible biosensors," *Mater. Lett.*, vol. 221, pp. 228–231, Jun. 2018, doi: 10.1016/j.matlet.2018.03.114.

[9] P. B. Johnson and R. W. Christy, "Optical constants of the noble metals," *Phys. Rev. B, Condens. Matter*, vol. 6, no. 12, pp. 4370–4379, Dec. 1972, doi: 10.1103/PhysRevB.6.4370.

[10] F. Schneider, J. Draheim, R. Kamberger, and U. Wallrabe, "Process and material properties of polydimethylsiloxane (PDMS) for optical MEMS," *Sens. Actuators A, Phys.*, vol. 151, no. 2, pp. 95–99, Apr. 2009, doi: 10.1016/j.sna.2009.01.026.

[11] B. P. Nelson, A. G. Frutos, J. M. Brockman, and R. M. Corn, "Near-infrared surface plasmon resonance measurements of ultrathin Films. 1. Angle shift and SPR imaging experiments," *Anal. Chem.*, vol. 71, no. 18, pp. 3928–3934, Sep. 1999.

[12] S. Pechprasarn and N. Albutt, "Multiple reflections modeling for multi-layered optical structures," *Appl. Mech. Mater.*, vol. 891, pp. 299–303, May 2019.

[13] I. Schwarz, N. Livneh, and R. Rapaport, "General closed-form condition for enhanced transmission in subwavelength metallic gratings in both TE and TM polarizations," *Opt. Exp.*, vol. 20, no. 1, pp. 426–439, 2012.

[14] M. Abutoama and I. Abdulhalim, "Self-referenced biosensor based on thin dielectric grating combined with thin metal film," *Opt. Exp.*, vol. 23, no. 22, pp. 28667–28682, 2015.

[15] M. Moharam, D. A. Pommet, E. B. Grann, and T. Gaylord, "Stable implementation of the rigorous coupled-wave analysis for surface-relief gratings: Enhanced transmittance matrix approach," *JOSA A*, vol. 12, no. 5, pp. 1077–1086, 1995.

[16] S. Pechprasarn, S. Learkthanakhachon, G. Zheng, H. Shen, D. Y. Lei, and M. G. Somekh, "Grating-coupled otto configuration for hybridized surface phonon polariton excitation for local refractive index sensitivity enhancement," *Opt. Exp.*, vol. 24, no. 17, pp. 19517–19530, 2016.

[17] P. Lalanne, J. P. Hugonin, and P. Chavel, "Optical properties of deep lamellar gratings: A coupled bloch-mode insight," *J. Lightw. Technol.*, vol. 24, no. 6, pp. 2442–2449, Jun. 2006.

[18] D. George *et al.*, "Coupling of surface plasmon polariton in al-doped ZnO with Fabry–Pérot resonance for total light absorption," *Photonics*, vol. 4, no. 4, p. 35, Apr. 2017.

[19] Y. Liang, W. Peng, R. Hu, and H. Zou, "Extraordinary optical transmission based on subwavelength metallic grating with ellipse walls," *Opt. Exp.*, vol. 21, no. 5, pp. 6139–6152, Mar. 2013.

[20] C. J. Chang-Hasnain and W. Yang, "High-contrast gratings for integrated optoelectronics," *Adv. Opt. Photon.*, vol. 4, no. 3, pp. 379–440, 2012.

[21] J. N. Polky and G. L. Mitchell, "Metal-clad planar dielectric waveguide for integrated optics," *JOSA*, vol. 64, no. 3, pp. 274–279, 1974.

[22] S.-W. Chang, T.-R. Lin, and S. L. Chuang, "Theory of plasmonic Fabry–Pèrot nanolasers," *Opt. Exp.*, vol. 18, no. 14, pp. 15039–15053, 2010.

[23] M. L. Povinelli *et al.*, "Evanescent-wave bonding between optical waveguides," *Opt. Lett.*, vol. 30, no. 22, pp. 3042–3044, 2005.

[24] N. Ismail, C. C. Kores, D. Geskus, and M. Pollnau, "Fabry-Pérot resonator: Spectral line shapes, generic and related airy distributions, linewidths, finesses, and performance at low or frequency-dependent reflectivity," *Opt. Exp.*, vol. 24, no. 15, pp. 16366–16389, 2016.

[25] L. Tu, L. Huang, and W. Wang, "A novel micromachined Fabry–Pèrot interferometer integrating nano-holes and dielectrophoresis for enhanced biochemical sensing," *Biosensors Bioelectron.*, vol. 127, pp. 19–24, Feb. 2019, doi: 10.1016/j.bios.2018.12.013.

[26] M. Bitarafan and R. DeCorby, "On-chip high-finesse Fabry–Pèrot microcavities for optical sensing and quantum information," *Sensors*, vol. 17, no. 8, p. 1748, Jul. 2017.

[27] P. Suvarnaphaet and S. Pechprasarn, "Enhancement of long-range surface plasmon excitation, dynamic range and figure of merit using a dielectric resonant cavity," *Sensors*, vol. 18, no. 9, p. 2757, Aug. 2018. [Online]. Available: https://www.mdpi.com/1424-8220/18/9/2757

[28] M. J. Dodge, "Refractive properties of magnesium fluoride," *Appl. Opt.*, vol. 23, no. 12, pp. 1980–1985, 1984.

[29] D. Franta, D. Nečas, and I. Ohlídal, "Universal dispersion model for characterization of optical thin films over a wide spectral range: Application to Hafnia," *Appl. Opt.*, vol. 54, no. 31, pp. 9108–9119, 2015.

[30] N. Sidqi, C. Clark, G. S. Buller, G. K. V. Thalluri, J. Mitrofanov, and Y. Noblet, "Comparative study of dielectric coating materials for microcavity applications," *Opt. Mater. Exp.*, vol. 9, no. 8, pp. 3452–3468, 2019.

[31] V. Karagodsky and C. J. Chang-Hasnain, "Physics of near-wavelength high contrast gratings," *Opt. Exp.*, vol. 20, no. 10, pp. 10888–10895, May 2012.

[32] Y. Zhai, G. Chen, J. Xu, Z. Qi, X. Li, and Q. Wang, "Multiple-band perfect absorbers based on the combination of Fabry–Pèrot resonance and the gap plasmon resonance," *Opt. Commun.*, vol. 399, pp. 28–33, Sep. 2017.

[33] R. Gupta, M. J. Dyer, and W. A. Weimer, "Preparation and characterization of surface plasmon resonance tunable gold and silver films," *J. Appl. Phys.*, vol. 92, no. 9, pp. 5264–5271, Nov. 2002.

[34] *E-Beam Resist AR-P 672 Series—Allresist EN*. Accessed: Feb. 6, 2021. [Online]. Available: https://www.allresist.com/portfolio-item/e-beam-resist-ar-p-672-series/

[35] K. Hosokawa, K. Hanada, and R. Maeda, "A polydimethylsiloxane (PDMS) deformable diffraction grating for monitoring of local pressure in microfluidic devices," *J. Micromech. Microeng.*, vol. 12, no. 1, pp. 1–6, Jan. 2002.

[36] A. A. A. Elfaki, R. A. Elobaid, A. A. Elamin, and M. D. Abd-Alla, "The effect of temperature and laser type on optical fiber temperature coefficient," *Amer. J. Opt. Photon.*, vol. 5, no. 1, pp. 1–5, 2017.

[37] S. Pechprasarn, B. Zhang, D. Albutt, J. Zhang, and M. Somekh, "Ultrastable embedded surface plasmon confocal interferometry," *Light, Sci. Appl.*, vol. 3, no. 7, pp. e187, Jul. 2014, doi: 10.1038/lsa.2014.68.

[38] Y. Yin, Y. Xia, X. Li, X. Yang, S. Xu, and J. Yin, "Narrow-linewidth and stable-frequency light source for laser cooling of magnesium fluoride molecules," *Appl. Phys. Exp.*, vol. 8, no. 9, Sep. 2015, Art. no. 092701.

[39] K. Lin, Y. Lu, Z. Luo, R. Zheng, P. Wang, and H. Ming, "Numerical and experimental investigation of temperature effects on the surface plasmon resonance sensor," *Chin. Opt. Lett.*, vol. 7, no. 5, pp. 428–431, 2009.

[40] C. Markos, K. Vlachos, and G. Kakarantzas, "Bending loss and thermo-optic effect of a hybrid PDMS/silica photonic crystal fiber," *Opt. Exp.*, vol. 18, no. 23, pp. 24344–24351, Nov. 2010.

[41] C. S. Moreira, A. M. N. Lima, H. Neff, and C. Thirstrup, "Temperature-dependent sensitivity of surface plasmon resonance sensors at the gold–water interface," *Sens. Actuators B, Chem.*, vol. 134, no. 2, pp. 854–862, Sep. 2008.

[42] Z. Gao *et al.*, "A facile PDMS coating approach to room-temperature gas sensors with high humidity resistance and long-term stability," *Sens. Actuators B, Chem.*, vol. 325, Dec. 2020, Art. no. 128810.

[43] S. Liu, Y. Ji, L. Cui, W. Sun, J. Yang, and H. Li, "Humidity-insensitive temperature sensor based on a quartz capillary anti-resonant reflection optical waveguide," *Opt. Exp.*, vol. 25, no. 16, pp. 18929–18939, 2017.

[44] P. E. Ciddor, "Refractive index of air: New equations for the visible and near infrared," *Appl. Opt.*, vol. 35, no. 9, pp. 1566–1573, 1996, doi: 10.1364/AO.35.001566.

[45] H. P. Ho *et al.*, "Sensitivity enhancement based on application of multi-pass interferometry in phase-sensitive surface plasmon resonance biosensor," *Opt. Commun.*, vol. 275, no. 2, pp. 491–496, Jul. 2007.

Suejit Pechprasarn was born in Bangkok, Thailand, in 1985. He received the B.Eng. degree in electronic and computer engineering from the University of Nottingham, U.K., in 2007, the B.Eng. degree in electrical engineering from Thammasat University, Thailand, in 2007, the Ph.D. degree in electrical and electronic engineering from the University of Nottingham in 2012, and the L.L.B. degree in Thai law from Ramkhamhaeng University, Thailand, in 2013.

From 2012 to 2014, he was a Research Assistant and a Research Fellow with the Institute of Biophysics, Imaging and Optical Science. From 2014 to 2018, he was a Senior Research Fellow with the Department of Electronic and Information Engineering, The Hong Kong Polytechnic University. In 2015, he was a Lecturer and an Associate Dean of Research and Innovation with the College of Biomedical Engineering, Rangsit University, Thailand. He has recently been promoted to an Associate Professor and an Associate Dean Emeritus. Since 2018, he has also been appointed as an Assistant Professor with the Nanophotonics Research Centre, Shenzhen University, Shenzhen, Guangdong, China.

Prof. Pechprasarn is a Peer Reviewer of the Optical Society of America (OSA) and the Springer and Nature Publishing Group. He is also a Research Proposal Reviewer of the National Science Centre, Poland, and the Committee of the Association of Researchers of Thailand.

Michael G. Somekh received the bachelor's degree in metallurgy and science of materials from Oxford University and the Ph.D. degree in microwave electronics from Lancaster University, U.K. After research fellowships at Oxford University, his first academic position was with University College London. He then joined the University of Nottingham, Nottingham, U.K., where he founded the Applied Optics Group. After a period working in Hong Kong, he joined Shenzhen University, as a Distinguished Professor and holds the part-time position with Nottingham University, as a Professor of Optical Engineering. His research interests include imaging, sensors, and ultrasonics. He is a Fellow of the Institute of Physics and was elected as a Fellow of the Royal Academy of Engineering (the U.K. National Engineering Academy) in 2012, in recognition of his interdisciplinary work.

Suvicha Sasivimolkul was born in Bangkok, Thailand, in 1996. He received the B.Eng. degree in biomedical engineering from the King Mongkut's Institute of Technology Ladkrabang, Thailand, in 2018. He is currently pursuing the master's degree in biomedical engineering with Rangsit University, which is focused on the development of optical sensors.